

DWRSeg: Dilation-wise Residual Network for Real-time Semantic Segmentation

Haoran Wei, Xu Liu, Shouchun Xu, Zhongjian Dai, Yaping Dai, Xiangyang Xu*

Beijing Institute of Technology

No. 5, South Street, Zhongguancun, Haidian District, Beijing

{hrwei, liuxu, 3220200814, daizhj, daiyaping, xxy1970}@bit.edu.cn

Abstract

Real-time semantic segmentation has played an important role in intelligent vehicle scenarios. Recently, numerous networks have incorporated information from multi-size receptive fields to facilitate feature extraction in real-time semantic segmentation tasks. However, these methods preferentially adopt massive receptive fields to elicit more contextual information, which may result in inefficient feature extraction. We believe that the elaborated receptive fields are crucial, considering the demand for efficient feature extraction in real-time tasks. Therefore, we propose an effective and efficient architecture termed Dilation-wise Residual segmentation (DWRSeg), which possesses different sets of receptive field sizes within different stages. The architecture involves (i) a Dilation-wise Residual (DWR) module for extracting features based on different scales of receptive fields in the high level of the network; (ii) a Simple Inverted Residual (SIR) module that uses an inverted bottleneck structure to extract features from the low stage; and (iii) a simple fully convolutional network (FCN)-like decoder for aggregating multiscale feature maps to generate the prediction. Extensive experiments on the Cityscapes and CamVid datasets demonstrate the effectiveness of our method by achieving a **state-of-the-art** trade-off between accuracy and inference speed, in addition to being lighter weight. Without using pretraining or resorting to any training trick, we achieve 72.7% mIoU on the Cityscapes test set at a speed of 319.5 FPS on one NVIDIA GeForce GTX 1080 Ti card, which is significantly faster than existing methods. The code and trained models are publicly available.

1. Introduction

As a basic task of computer vision, semantic segmentation aims to label each pixel with semantics and plays a significant role in many fields, including automatic driving, robot sensing, satellite remote sensing, video surveillance,

*Corresponding author.

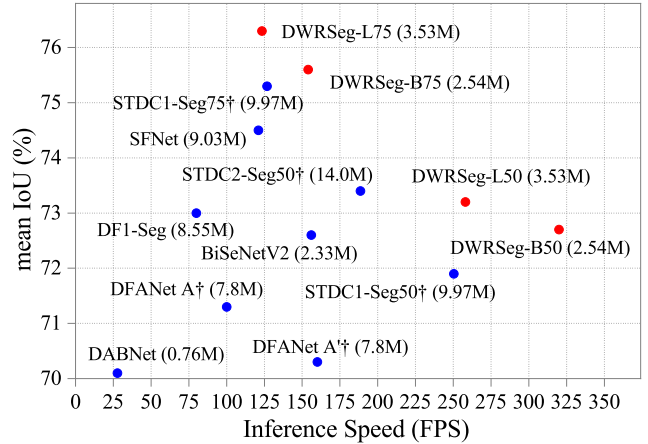


Figure 1. Speed-accuracy performance comparison on the Cityscapes test set. Our methods are presented as red dots, while the other methods are presented as blue dots. † represents the methods pretrained on ImageNet. The parameters of the methods are shown in parentheses. Our approaches achieve a state-of-the-art speed-accuracy trade-off.

and medical imaging.

To achieve a satisfactory trade-off between inference speed and accuracy, researchers continue to pursue the design of more lightweight and efficient networks. These efforts are mainly concentrated in two directions. One focuses on designing more efficient decoders to fuse feature maps from the encoder. These studies [10–12, 24] usually borrow lightweight backbones from image classification as the encoder, achieving fair performance on various benchmarks. However, these methods have limited effects due to the difference between classification and segmentation tasks.

Another direction develops specialized backbones, in which many works have made notable contributions. Two main styles of structures were developed to obtain scalable receptive fields for feature extraction. Some methods [7, 23] vertically stacked 3×3 convolutions to gradually acquire a large receptive field, while others [9, 21] used parallel dilated convolutions to directly obtain a large receptive field.

All these methods tend to utilize massive receptive fields to obtain more contextual information, promoting the effect of feature extraction. However, we observe that excessive receptive fields may lead to low feature extraction efficiency. Therefore, we hold the view that the elaborated receptive field size is an indispensable guarantee of the high feature extraction efficiency, which constrains the computational cost and improves the feature representation for real-time semantic segmentation.

To this end, we propose a novel architecture for real-time semantic segmentation, focusing on the design of the receptive field for feature extraction. First, a Dilation-wise Residual (DWR) module is introduced for extracting features at the high level of the network, as shown in Figure 2a. A multibranch structure is used to expand the receptive field, where each branch adopts a dilated depth-wise convolution at a different rate. Then, a Simple Inverted Residual (SIR) module is specifically designed to extract features at the low level of the network, as shown in Figure 2b. This module only possesses a tiny receptive field of 3×3 but uses a structure in an inverted bottleneck style to expand the number of channels, securing stronger feature extraction capability. Finally, based on the DWR and SIR modules, an encoder-decoder style network—DWRSeg—is constructed, as shown in Figure 5, in which the decoder adopts a simple FCN-like [13] structure. The decoder directly upsamples the feature maps with strong semantic information from the last two stages and then concatenates them with the feature maps from the lower stage, which contain rich detailed information, for final prediction.

Our main contributions can be summarized as follows:

- We propose a novel DWR module with a multibranch structure for feature extraction from a scalable receptive field at the high levels of the network;
- We design an SIR module in an inverted bottleneck style to enhance the feature extraction ability at the low level of the network;
- Based on the DWR and SIR modules, an encoder-decoder style network, DWRSeg, is constructed, which uses a fairly simple FCN-like decoder to aggregate semantic and detailed features;
- We conduct extensive experiments to verify the effectiveness of our methods, and our architecture achieves impressive results on Cityscapes, as shown in Figure 1. Specifically, we obtain 72.6% mIoU on the Cityscapes test set at a speed of 322.1 FPS on one NVIDIA GeForce GTX 1080 Ti card.

2. Related Work

2.1. Real-time Semantic Segmentation

Real-time semantic segmentation networks have attracted much attention because of the growing demand for practical applications. These models can be divided into 3 categories according to the adopted backbones [16]. (i) *lightweight classification model-based method*. The DFANet [10] utilizes a modified Xception [5] model as the backbone and aggregates features in a cascaded manner. The SFNet [11] adopts the ResNet [8], ShuffleNet V2 [15] and DF [12] series as the backbone in the encoder and proposes a FAM to learn semantic flow in the decoder. The BiSeNetV1 [24] uses Xception39 [5] as the backbone of the context path and designs a feature fusion module (FFM) to merge features. (ii) *multibranch architecture-based method*. The ICNet [26] takes cascaded images into multiresolution branches and utilizes a cascade feature fusion unit to quickly carry out high-quality segmentation. BiSeNetV2 [23] uses two branches to obtain semantic and detail information; then, it fuses both types of feature representations through a guided aggregation layer. (iii) *specialized backbone-based method*. The ENet [17] employs a special initial block and several bottleneck blocks to make up the backbone. The first two blocks heavily reduce the input size to avoid expensive computation. The DABNet [9] utilizes a novel depth-wise asymmetric bottleneck (DAB) module to construct the backbone, which is able to create a sufficient receptive field and densely utilize the contextual information.

2.2. Receptive Field

The design of the receptive field is of great importance for real-time semantic segmentation networks since it is related to both speed and accuracy. [14] showed that the effective receptive field only accounts for a fraction of the full theoretical receptive field. DeepLab V2 [2] uses an atrous spatial pyramid pooling (ASPP) module composed of parallel convolutions with different receptive fields to extract different features, thus capturing image context information at multiple scales. Following DeepLab V2, many algorithms [3, 4, 22, 27] have achieved advanced performance by using ASPP-like modules at the bottom of the backbone. Different from the above, some works [20, 21, 25] explored designing multiscale receptive field modules and interspersing them in a specialized backbone. In this paper, we propose an efficient lightweight backbone to provide a scalable receptive field.

3. Proposed Method

In this section, we first set forth our design motivation of the network and then introduce our core modules, referred

to as the DWR module and SIR module. Finally, the architecture of the entire network for real-time semantic segmentation is presented.

3.1. Design Motivation

Many recent approaches [7, 9, 21] have designed dedicated backbones for real-time semantic segmentation tasks, of which the design of the receptive field is an important part. Generally, these methods pursue vast receptive fields to capture more contextual information, thus promoting feature representation ability. However, we believe that in practice, this may lead to inefficient feature extraction. [9, 21] use dilated convolutions with massive dilation rates at the high layers of their networks, but we observe that barely any parameter in these convolutions can be learnt. The reason for this phenomenon is that it is scarcely possible for such convolutions to establish connections between features over a substantially large spatial span directly, leading to low feature extraction efficiency. While [7] keeps the same receptive field size throughout the network, which is too large for low-level feature extraction, thus limiting the efficiency. We observe that at the low level of [7], fewer convolution layers but more channels can produce better results.

We deem that it is essential to identify an appropriate receptive field size to improve the efficiency of feature extraction, and the requirements for receptive field size are different within different stages of the network. With the enhancement of the feature semantic representation, higher stages require a larger receptive field. Therefore, a module using dilated convolutions to expand the receptive fields and a module using a regular convolution to limit the receptive fields are designed for the higher and low stages, respectively. Furthermore, we believe that the requirements for different sizes of receptive fields at one layer are also different. Specifically, dilated convolutions with a small dilation rate are always important, because intermediate features are required to establish connections between features with large spatial distances. Accordingly, a multibranch structure with dilated convolutions of various receptive fields is adopted in our module, and each branch holds a different channel capacity. Ultimately, we propose DWR and SIR modules to construct our encoder.

3.2. Dilation-wise Residual Module

The core of our work lies in the design of the DWR module for feature extraction.

Module Structure. According to the above analysis, we designed the feature extraction module structure shown in Figure 2a, which is applied in the high level of the network. A multibranch structure is used to adapt to the requirements for various sizes of receptive fields in one layer. For each branch, a common convolution with a 3×3 ker-

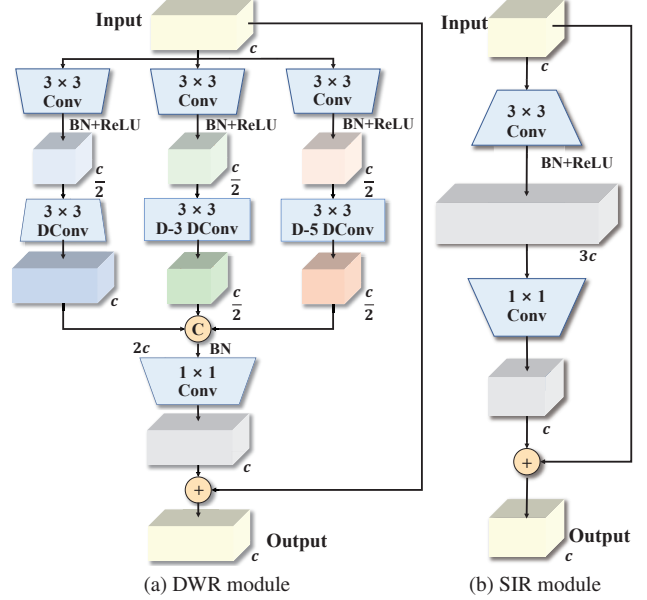


Figure 2. Illustration of the structure of the DWR module and SIR module. (a) and (b) present the DWR module of the three-branch structure for the high-level network and the SIR module of the single-path structure for the low-level network, respectively. Conv denotes convolution, DConv denotes depth-wise convolution, D- n denotes dilated convolution with a dilation rate of n , C in a circle denotes the concatenate operation, + in a circle denotes the addition operation, and c denotes the base number of feature map channels.

nel, combined with a batch normalization (BN) layer and ReLU layer, is employed to extract features first. We name this step region-residualization. Since each output channel contains several small spatial regions that need to be refined, the entire output is a set of all these regions. Then, a dilated depth-wise 3×3 convolution follows to extract semantic information from these regions. Feature maps then pass through a BN layer to obtain semantic residuals. This operation is named semantic-residualization, which further analyses semantic information from regional features. The visualized features in region-residualization and semantic-residualization are shown in Figure 3. Then, feature maps are concatenated from all branches, and a point-wise convolution is used to merge all the feature maps, generating final residuals corresponding to the input feature maps. Last, the final residuals are added to the input feature maps to construct a stronger and more comprehensive feature representation.

In addition, the features extracted with a small receptive field are relatively important regardless of the stage; therefore, the number of dilated depth-wise convolution channels with the lowest rate is set to twice the other channels. According to the characteristics of combining features from

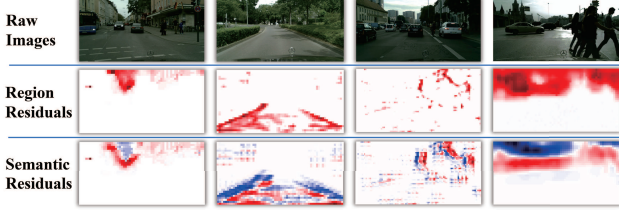


Figure 3. Illustration of the visualized heatmap of features in region-residualization and semantic-residualization. The upper row shows the raw images. The middle row shows feature maps obtained by region-residualization. This operation can activate some spatial regions. The lower row shows the corresponding feature maps obtained by semantic-residualization. This operation further analyses semantic information from the regional features.

dilated convolutions with various rates as well as the residual structure, the module is named the DWR module.

Design Details. Although the structure of the module is uncomplicated, there are some details worth noting. First, compared with other multibranch modules, such as the CG block [21], the beginning convolution (region-residualization) stands in all branches rather than before branches, producing unshared regions for each branch. The unshared region-residualization is crucial since regions for semantic-residualization that need different receptive field sizes may differ from each other. Second, the nonlinearity in the DWR module is relatively low compared with other residual blocks (such as the CG block [21], the DAB module [9] and the GE layer [23]). Excessive nonlinearity may not yield better results, but it may lead to inefficiency. Therefore, only two BN layers and one ReLU layer are utilized in one DWR module.

Overall, the formulation of the DWR module for the top-most stage is shown in Equation (1):

$$\begin{aligned} C_1(x) &= \text{ReLU}(\text{BN}(\text{Conv}(x))) \\ C_2(x, d) &= D_d \text{DCConv}(C_1(x)) \\ \text{DWR}(x) &= \text{PConv}(\text{BN}(\Gamma_d\{C_2(x, d)\})) + x, \end{aligned} \quad (1)$$

where x denotes the input feature maps, $\text{Conv}(\cdot)$ denotes 3×3 common convolutions, $D_d \text{DCConv}(\cdot)$ denotes dilated depth-wise 3×3 convolutions with dilation rate d , $\text{PConv}(\cdot)$ denotes point-wise convolutions, and $\Gamma_d\{\cdot\}$ denotes concatenation operations for all d .

3.3. Simple Inverted Residual Module

Based on the design idea that the requirements for the large sizes of the receptive field in the low level are relatively low, a dedicated module, the SIR module, is designed for feature extraction in the low stage, as shown in Figure 2b. Compared with the DWR module, there are three modifications: (i) only one branch is adopted to reduce the

size of the receptive field; (ii) the 3×3 depth-wise convolution is abandoned to further limit the receptive field in the entire module; (iii) channel expansion is employed to fortify the feature extraction ability; specifically, the beginning convolution expands the number of channels of the input to three times. Then, as with the DWR module, a point-wise convolution is used to merge channels. The style of this proposed module is similar to that of the inverted residual block in MobileNet v2 [18]. However, our module is simpler because only two convolution layers are utilized; therefore, we name this module the SIR module. The formulation of the SIR module is shown in Equation (2):

$$\begin{aligned} C_1(x) &= \text{ReLU}(\text{BN}(\text{Conv}(x))) \\ \text{SIR}(x) &= \text{PConv}(C_1(x)) + x \end{aligned} \quad (2)$$

3.4. Network Architecture

The whole architecture is shown in Figure 5. In general, our proposed network is in an encoder-decoder fashion. The encoder contains four stages, and the decoder adopts a simple FCN-like structure.

Encoder. Following BiSeNetV2 [23], a stem block is adopted as the first stage of our network, as shown in Figure 4a. Two adjustments are made to the stem block presented in BiSeNetV2. First, we remove the activation layer for the first convolution to retain more valid information from the original pictures. Then, the last convolution does not perform feature shrinkage. This structure has low computational cost and effective feature expression ability.

Stage 2 is composed of SIR modules, which produce high-resolution feature maps with abundant detailed information. Stages 3 and 4 both consist of DWR modules, which generate features with strong semantic information. For stage 4, three-branch DWR modules with dilation rates set to 1, 3, and 5 are employed, while the third branch is abandoned for stage 3. Within the last three stages, the first module in each stage undertakes downsampling by adjusting the first convolution with a stride of 2.

Decoder. The decoder adopts a simple FCN-like structure, as shown in Figure 5. The output feature maps of stages 3 and 4 are first upsampled and then concatenated with feature maps from stage 2. After that, a BN layer acts on the concatenated feature maps. Finally, a segmentation head (SegHead) is used for prediction. The structure of the SegHead is illustrated in Figure 4b. A 3×3 convolution with a BN layer and an ReLU layer is set to merge the feature maps. Afterwards, a point-wise convolution is used for prediction. The feature maps are upsampled to the input size in the end. The formulation of the decoder is shown in Equation (3):

$$\begin{aligned} C_1(f_s) &= \Gamma\{\text{Up}_4(f_h), \text{Up}_2(f_m), f_l\} \\ C_2(f_s) &= \text{ReLU}(\text{BN}(\text{PConv}(f_s))) \\ \text{Decoder}(f_s) &= \text{Up}_8(\text{PConv}(C_2(f_s))) \end{aligned} \quad (3)$$

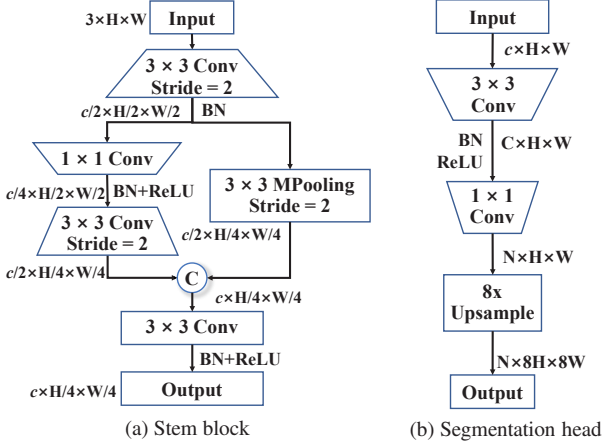


Figure 4. Illustration of the structure of the stem block and Seg-Head. (a) presents the structure of the stem block, which is used to process the input images; (b) presents the structure of the Seg-Head, which is used to convert feature maps into the final prediction. Conv denotes convolution, Mpooling denotes the max pooling, C in a circle denotes the concatenate operation, c denotes the base number of feature map channels, and H and W denote the input size.

where f_h, f_m, f_l denote feature maps from stages 4, 3, and 2, respectively, f_s denotes (f_h, f_m, f_l) , and Up_i denotes the upsampling operation for i number of steps. The output of the decoder is then directly supervised by the ground truth. We adopt cross-entry loss with Online Hard Example Mining [19] to optimize the semantic segmentation learning task.

We carefully tune the hyperparameters in the whole network until the best trade-off between accuracy and efficiency is reached. Finally, we report two versions: DWRSeg-Base (DWRSeg-B) and DWRSeg-Large (DWRSeg-L). Table 1 shows the detailed structure of our DWRSeg networks.

4. Experiments

In this section, we first introduce the experimental settings. Next, we investigate our design idea and the effects of each component of our proposed approach on the Cityscapes test set. Finally, we report our accuracy and speed results on different benchmarks compared with those of other algorithms.

4.1. Experimental Settings

Datasets. Cityscapes [6] is an urban street scenes semantic segmentation dataset. It contains training, validation and test sets, with 2,975, 500 and 1,525 annotated images, respectively. The resolution of the images is $2,048 \times 1,024$. Only 19 classes are used for semantic segmentation task.

The Cambridge-driving Labeled Video Database

Stages	R	C	B	Repetitions	
				DWRSeg-B	DWRSeg-L
Image	1	3			
Stem block	1/4	64			
SIR modules	1/8	64	1	7	8
DWR modules	1/16	128	2	3	8
DWR modules	1/32	128	3	3	3
Decoder cat	1/8	320			
Decoder conv1	1/8	128			
Decoder conv2	1/8	N			
Flops				13.62G	16.42G
Params				2.54M	3.53M

Table 1. Detailed architecture of DWRSeg networks. R, C and B denote the ratio between the output size and input image size, output channels and branch number of the module respectively; FLOPS are estimated for an input resolution of $3 \times 512 \times 1024$; N denotes the number of classes.

(CamVid) [1] is a road scene dataset taken from the perspective of a driving automobile. All images have a resolution of 960×720 and are split into 367 images for training, 101 images for validation and 233 images for testing. Only 11 classes is involved in our experiments for a fair comparison with other methods.

Evaluation Metrics. We adopt the the mean intersection over union (mIoU) and frames per second (FPS) as the evaluation metrics for testing the accuracy and speed, respectively.

Implementation Details. For training, we use mini-batch stochastic gradient descent (SGD) with 0.9 momentum and 0.0005 weight decay to train our model. For all datasets, the batch size is set as 16. As a common configuration, we utilize a 'poly' learning rate policy in which the initial rate is multiplied by $(1 - \frac{iter}{maxiter})^{power}$. The power is set to 0.9, and the initial learning rate is set as 0.02. In addition, we train the models for 1,000 and 600 epochs for the Cityscapes and CamVid datasets, respectively.

Data augmentation includes color jittering, random horizontal flipping, random cropping and random resampling. The resize scale range is $[0.25, 1.5]$, and the cropped resolution is 1280×640 for training Cityscapes. For CamVid, the resize scale range is $[0.5, 1.5]$, and the cropped resolution is

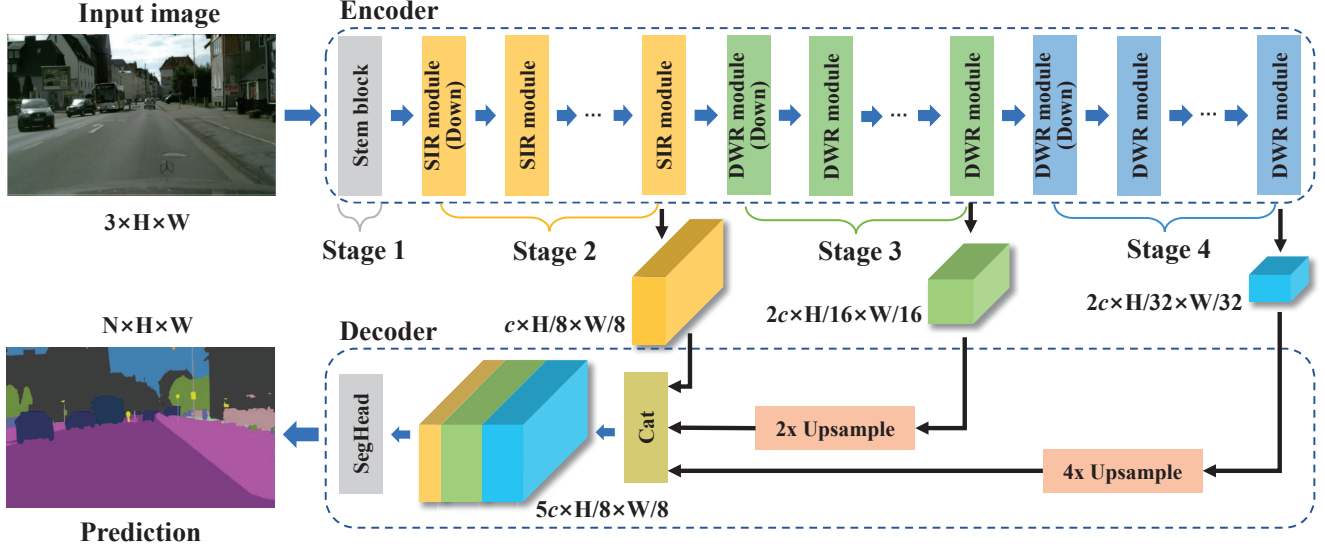


Figure 5. Illustration of the structure of the entire network. The structure is relatively simple; it is a typical encoder-decoder style. The encoder includes four stages, which are composed of a stem block, SIR modules, DWR modules (2 branches) and DWR modules (3 branches). The stem block is used for initial processing, the SIR modules are used to extract features from the low stage, and the DWR modules are used to extract features from the higher stages. The output of the upper three layers enters the decoder, which is a simple FCN-like style. Feature maps from the higher stages are first upsampled and then concatenated with feature maps from the lower stage. Finally, a SegHead is used to process the concatenated feature maps to conduct the final prediction. H and W denote the input image size, N denotes the number of classes, and c denotes the base number of feature map channels.

960×720 .

All our networks are trained **without pretraining on ImageNet**.

For inference, we do not adopt any evaluation tricks, e.g., sliding-window evaluation and multiscale testing, which can improve accuracy but are time consuming. For Cityscapes, we first resize images to 1024×512 or 1536×768 to perform the inference and then resize the prediction to the original image size.

We conduct all our experiments based on PyTorch-1.10, CUDA 11.3, CUDNN 8.2.0 and TensorRT 8.2.3.0. Two NVIDIA RTX 3090 GPUs are used for training, and the measurement of inference time is executed on an NVIDIA GTX 1080Ti GPU with a batch size of 1 for benchmarking.

4.2. Experiments on Our Design Idea

We design an experiment to verify our design concept and test how much receptive field is needed specifically for each stage of the network. A special module is built for this experiment, whose structure is shown in Figure 6. In this module, all branches share one region-residualization so that all semantic-residualizations with different receptive field sizes compete for regional features. We replace all DWR modules and SIR modules in DWRSeg-L with this module and then observe the weights in point-wise convolution corresponding to each branch; we use this to determine the importance of different receptive field sizes for

the current stage. The probability mass function (PMF) and the cumulative distribution function (CDF) of weights of each branch in different stages are shown in Figure 7. The convolution weights responsible for features from the small receptive field in the low stage are much greater than the others. In the middle stage, the weights for the larger receptive field increase considerably, while those for the small receptive field remain the greatest. In regard to the high stage, the weights for the largest receptive field are almost the same as those for the small. Therefore, we can conclude that from the low level to the high level, the demand for the wider receptive field grows. However, even at the top-most stage, the demand for a small receptive field size has not decreased significantly. Consequently, this experiment verifies that our design idea is reasonable.

4.3. Ablation Studies

This section introduces the ablation experiments to validate the effectiveness of each component in our method. To eliminate the influence of different model sizes, except for the last ablation experiment, the number of modules in all models was adjusted to a similar inference speed.

Unshared Region-Residualization in the DWR Module. Table 2 Expt. 1 illustrates the results of unshared region-residualization ('w') and shared region-residualization ('w/o') in the DWR module. The results show that unshared region-residualization provides a vast

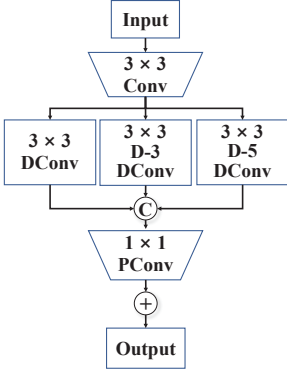


Figure 6. Illustration of the designed module to test the demand for receptive fields, whose branches share the same region-residualization.

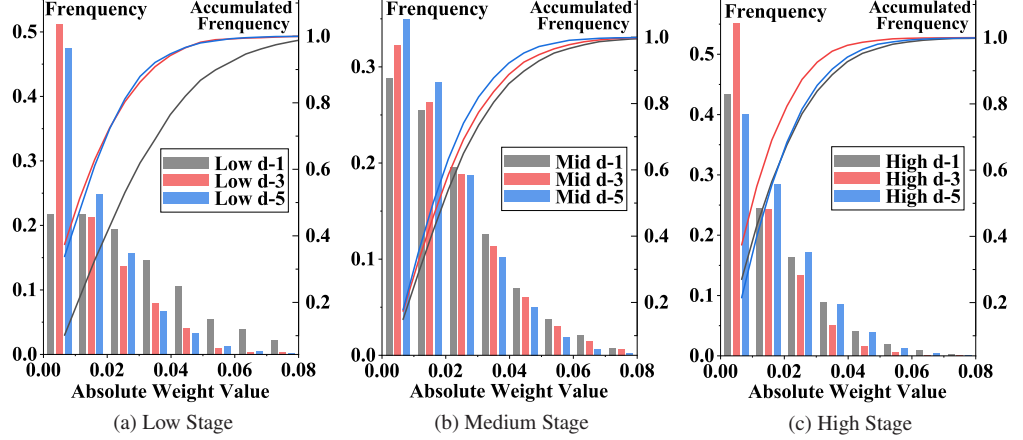


Figure 7. Illustration of the probability mass function (PMF) and cumulative distribution function (CDF) of the absolute weights in point-wise convolution corresponding to each branch of the top three stages. (a), (b) and (c) present the PMF and CDF of the low, medium and high stages, respectively. The histograms show the PMF, and the curves show the CDF. Gray, blue and red represent the absolute weights corresponding to the branches with dilation rates of 1, 3 and 5, respectively.

improvement in the output.

Ratios of Different Receptive Fields in the DWR module. Table 2 Expt. II investigates the effects of different ratios α of the output channel numbers of the three branches (d-1:d-3:d-5) in the DWR module. When we adjust α , the best effect is obtained when the ratio is 2:1:1.

Channel Number of Region-Residualization in the DWR Module. Table 2 Expt. III shows the results of setting a different ratio β of the output channel number to the input channel number of the region-residualization in the DWR module. The best output is achieved when β is set to 0.5.

Nonlinearity in the DWR Module. Table 2 Expt. IV illustrates the impact of different degrees of nonlinearity in the DWR module. Sitch 1 represents region-residualization without the ReLU, Sitch 2 represents region-residualization without BN, Sitch 3 represents semantic-residualization without BN, Sitch 4 represents adding an ReLU after BN in semantic-residualization and Sitch 5 represents adding a BN after point-wise convolution. The results show that when the nonlinearity is lower, the effect decreases considerably; however, increasing more nonlinearity does not improve the output.

Depth-wise Convolution in the SIR Module. As shown in Table 2 Expt. V, the improvement obtained by adding a depth-wise convolution with a BN layer ('w') is less than that obtained by increasing the number of modules ('w/o') in the SIR module.

Channel Expansion in the SIR Module. Table 2 Expt. VI shows the effects of expanding the channel number of the beginning convolution to λ times in the SIR module. When the number of channels expands to three times, the

best result is obtained.

Block Number. We adjust the number of modules and present the results in Table 2 Expt. VII. δ represents the module number offset to the baseline. Each column shows the results obtained when the number of modules in the corresponding stage changes according to δ , while the number of modules in other stages remains unchanged. The benefits of more blocks appreciably decrease, and a deeper network is detrimental to parallel calculation and FPS.

4.4. Comparison with State-of-the-Art Methods

In this section, we compare our best models (DWRSeg-B and DWRSeg-L) with other state-of-the-art methods on two datasets: Cityscapes and CamVid.

Results on Cityscapes. Table 3 presents the segmentation accuracy, inference speed and model parameters of our proposed method on the Cityscapes test set. Following the previous methods, we use the training set and validation set to train our models before submitting them to the Cityscapes online server. We use 50 and 75 after the method name to represent the input size 512×1024 and 768×1536 , respectively. Our DWRSeg-L75 achieves the best mIoU of 76.3% at 123.4 FPS, and our DWRSeg-B50 achieves the fastest speed of 319.5 FPS with an mIoU of 72.7%. Compared with the second-best model, the STDC, which uses pretraining and auxiliary segmentation, our models produce a **state-of-the-art** trade-off between accuracy and speed without using pretraining or resorting to any training trick. Moreover, our models are much lighter than STDC, with only a quarter of the STDC parameters.

Results on CamVid. Table 4 shows the comparison results with other methods. DWRSeg-B achieves 76.5%

Expt.	Method		mIoU(%)	FPS	
I	UR	w (B/L)	76.3	123.4	
		w/o	75.6	121.3	
II	α	2:1:1 (B/L)	76.3	123.4	
		1:1:1	76.0	121.8	
		3:1:1	75.6	123.4	
III	β	0.5 (B/L)	76.3	123.4	
		1	75.3	122.3	
IV	NL	B/L	76.3	123.4	
		Sitch 1	75.2	124.3	
		Sitch 2	75.0	127.8	
		Sitch 3	75.6	126.5	
		Sitch 4	76.2	120.3	
		Sitch 5	76.3	118.5	
V	PWC	w/o (B/L)	76.3	123.4	
		w	75.6	122.6	
VI	λ	1	76.3	123.4	
		2	75.8	121.8	
		3 (B/L)	75.7	123.4	
		4	75.7	123.4	
	Method	mIoU(%)			
		Stage 2	Stage 3	Stage 4	
VII	δ	-2	74.9	75.7	75.2
		-1	75.6	76	75.6
		0 (B/L)	76.3	76.3	76.3
		1	76.4	76.1	76.3

Table 2. Ablation experiments on the network structure design on Cityscapes. The baseline (B/L) method for all ablation experiments is the DWRSeg-L model, and all results are obtained under the input size of 1536×768 . UR denotes unshared region-residualization in the DWR module; α denotes the ratio of output channel numbers in three branches of the DWR module; β denotes the ratio of the output channel number to the input channel number of region-residualization in the DWR module; NL denotes nonlinearity; PWC denotes point-wise convolution in the SIR module; λ denotes the ratio of the output channel number to the input channel number of beginning convolution in the SIR module and δ denotes the block number offset to the baseline.

mIoU at 237.2 FPS and DWRSeg-L achieves 77.5% mIoU at 189.2 FPS. This further demonstrates the superior capability of our method.

5. Conclusions

In this paper, we propose the view that at different stages of the network, the requirements for the size of the receptive field are different, and they are also different within a specific layer. Therefore, a DWR module is designed for the high stages of the network; this module is capable of extracting features with different sizes of receptive fields by multibranch dilated convolutions. Then, an SIR mod-

Model	Input Ratio	mIoU (%)	FPS	Params (M)
ENet [17]	0.5	58.3	76.9	0.37
ICNet [†] [26]	1.0	69.5	30.3	26.5
DABNet [9]	1.0	70.1	27.7	0.76
DFANet B [†] [10]	1.0	67.1	120	4.8
DFANet A [†] [10]	1.0	71.3	100	7.8
BiSeNetV2 [23]	0.5	72.6	156	2.33
DF1-Seg [12]	1.0	73.0	80	8.55
DF2-Seg [12]	1.0	74.8	55	8.55
SFNet(DF1) [11]	1.0	74.5	121	9.03
STDC1-Seg50 [†] [7]	0.5	71.9	250.4	9.97
STDC2-Seg50 [†] [7]	0.5	73.4	188.6	14.0
STDC1-Seg75 [†] [7]	0.75	75.3	126.7	9.97
STDC2-Seg75 [†] [7]	0.75	76.8	97.0	14.0
DWRSeg-B50	0.5	72.7	319.5	2.54
DWRSeg-L50	0.5	73.1	256.2	3.53
DWRSeg-B75	0.75	75.6	151.7	2.54
DWRSeg-L75	0.75	76.3	123.4	3.53

Table 3. Comparisons with other state-of-the-art methods on Cityscapes. The base resolution is 1024×2048 . [†] means that the model is pretrained on ImageNet.

Model	mIoU(%)	FPS
ICNet [†] [26]	67.1	34.5
DFANet A [†] [10]	64.7	120
STDC1 [†] [7]	73.0	197.6
STDC2 [†] [7]	73.9	152.2
BiSeNetV2* [23]	76.7	124.5
DWRSeg-B*	76.5	237.2
DWRSeg-L*	77.5	189.2

Table 4. Comparisons with other state-of-the-art methods on CamVid. [†] means the models are pretrained on ImageNet; * means the models are pretrained on Cityscapes.

ule with a small receptive field is proposed for feature extraction in the low stage, which uses an inverted bottleneck structure to promote feature presentation abilities. Based on the DWR and the SIR modules, an encoder-decoder style network, DWRSeg, is constructed, whose decoder adopts a simple FCN-like structure. Extensive ablation experiments indicate the effectiveness of our proposed DWRSeg networks, and the comparison experiments with other networks demonstrate that our networks reach a state-of-the-art trade-off between accuracy and speed. Moreover, our networks are being lighter weight. We hope that the idea and structure of DWRSeg foster further research in semantic segmentation.

Acknowledgment. This research is supported by Beijing Municipal Natural Science Foundation (No. L191020).

References

- [1] Gabriel J Brostow, Jamie Shotton, Julien Fauqueur, and Roberto Cipolla. Segmentation and recognition using structure from motion point clouds. In *European conference on computer vision*, pages 44–57. Springer, 2008. 5
- [2] Liang-Chieh Chen, George Papandreou, Iasonas Kokkinos, Kevin Murphy, and Alan L Yuille. Deeplab: Semantic image segmentation with deep convolutional nets, atrous convolution, and fully connected crfs. *IEEE transactions on pattern analysis and machine intelligence*, 40(4):834–848, 2017. 2
- [3] Liang-Chieh Chen, George Papandreou, Florian Schroff, and Hartwig Adam. Rethinking atrous convolution for semantic image segmentation. *arXiv preprint arXiv:1706.05587*, 2017. 2
- [4] Liang-Chieh Chen, Yukun Zhu, George Papandreou, Florian Schroff, and Hartwig Adam. Encoder-decoder with atrous separable convolution for semantic image segmentation. In *Proceedings of the European conference on computer vision (ECCV)*, pages 801–818, 2018. 2
- [5] François Chollet. Xception: Deep learning with depthwise separable convolutions. In *Proceedings of the IEEE conference on computer vision and pattern recognition*, pages 1251–1258, 2017. 2
- [6] Marius Cordts, Mohamed Omran, Sebastian Ramos, Timo Rehfeld, Markus Enzweiler, Rodrigo Benenson, Uwe Franke, Stefan Roth, and Bernt Schiele. The cityscapes dataset for semantic urban scene understanding. In *Proceedings of the IEEE conference on computer vision and pattern recognition*, pages 3213–3223, 2016. 5
- [7] Mingyuan Fan, Shenqi Lai, Junshi Huang, Xiaoming Wei, Zhenhua Chai, Junfeng Luo, and Xiaolin Wei. Rethinking bisenet for real-time semantic segmentation. In *Proceedings of the IEEE/CVF conference on computer vision and pattern recognition*, pages 9716–9725, 2021. 1, 3, 8
- [8] Kaiming He, Xiangyu Zhang, Shaoqing Ren, and Jian Sun. Deep residual learning for image recognition. In *Proceedings of the IEEE conference on computer vision and pattern recognition*, pages 770–778, 2016. 2
- [9] Gen Li, Inyoung Yun, Jonghyun Kim, and Joongkyu Kim. Dabnet: Depth-wise asymmetric bottleneck for real-time semantic segmentation. *arXiv preprint arXiv:1907.11357*, 2019. 1, 2, 3, 4, 8
- [10] Hanchao Li, Pengfei Xiong, Haoqiang Fan, and Jian Sun. Dfanet: Deep feature aggregation for real-time semantic segmentation. In *Proceedings of the IEEE/CVF Conference on Computer Vision and Pattern Recognition*, pages 9522–9531, 2019. 1, 2, 8
- [11] Xiangtai Li, Ansheng You, Zhen Zhu, Houlong Zhao, Maoke Yang, Kuiyuan Yang, Shaohua Tan, and Yunhai Tong. Semantic flow for fast and accurate scene parsing. In *European Conference on Computer Vision*, pages 775–793. Springer, 2020. 1, 2, 8
- [12] Xin Li, Yiming Zhou, Zheng Pan, and Jiashi Feng. Partial order pruning: for best speed/accuracy trade-off in neural architecture search. In *Proceedings of the IEEE/CVF Conference on Computer Vision and Pattern Recognition*, pages 9145–9153, 2019. 1, 2, 8
- [13] Jonathan Long, Evan Shelhamer, and Trevor Darrell. Fully convolutional networks for semantic segmentation. In *Proceedings of the IEEE conference on computer vision and pattern recognition*, pages 3431–3440, 2015. 2
- [14] Wenjie Luo, Yujia Li, Raquel Urtasun, and Richard Zemel. Understanding the effective receptive field in deep convolutional neural networks. *Advances in neural information processing systems*, 29, 2016. 2
- [15] Ningning Ma, Xiangyu Zhang, Hai-Tao Zheng, and Jian Sun. Shufflenet v2: Practical guidelines for efficient cnn architecture design. In *Proceedings of the European conference on computer vision (ECCV)*, pages 116–131, 2018. 2
- [16] Yujian Mo, Yan Wu, Xinneng Yang, Feilin Liu, and Yujun Liao. Review the state-of-the-art technologies of semantic segmentation based on deep learning. *Neurocomputing*, 493:626–646, 2022. 2
- [17] Adam Paszke, Abhishek Chaurasia, Sangpil Kim, and Eugenio Culurciello. Enet: A deep neural network architecture for real-time semantic segmentation. *arXiv preprint arXiv:1606.02147*, 2016. 2, 8
- [18] Mark Sandler, Andrew Howard, Menglong Zhu, Andrey Zhmoginov, and Liang-Chieh Chen. Mobilenetv2: Inverted residuals and linear bottlenecks. In *Proceedings of the IEEE conference on computer vision and pattern recognition*, pages 4510–4520, 2018. 4
- [19] Abhinav Shrivastava, Abhinav Gupta, and Ross Girshick. Training region-based object detectors with online hard example mining. In *Proceedings of the IEEE conference on computer vision and pattern recognition*, pages 761–769, 2016. 5
- [20] Panqu Wang, Pengfei Chen, Ye Yuan, Ding Liu, Zehua Huang, Xiaodi Hou, and Garrison Cottrell. Understanding convolution for semantic segmentation. In *2018 IEEE winter conference on applications of computer vision (WACV)*, pages 1451–1460. Ieee, 2018. 2
- [21] Tianyi Wu, Sheng Tang, Rui Zhang, Juan Cao, and Yongdong Zhang. Cgnet: A light-weight context guided network for semantic segmentation. *IEEE Transactions on Image Processing*, 30:1169–1179, 2020. 1, 2, 3, 4
- [22] Maoke Yang, Kun Yu, Chi Zhang, Zhiwei Li, and Kuiyuan Yang. Denseaspp for semantic segmentation in street scenes. In *Proceedings of the IEEE conference on computer vision and pattern recognition*, pages 3684–3692, 2018. 2
- [23] Changqian Yu, Changxin Gao, Jingbo Wang, Gang Yu, Chunhua Shen, and Nong Sang. Bisenet v2: Bilateral network with guided aggregation for real-time semantic segmentation. *International Journal of Computer Vision*, 129(11):3051–3068, 2021. 1, 2, 4, 8
- [24] Changqian Yu, Jingbo Wang, Chao Peng, Changxin Gao, Gang Yu, and Nong Sang. Bisenet: Bilateral segmentation network for real-time semantic segmentation. In *Proceedings of the European conference on computer vision (ECCV)*, pages 325–341, 2018. 1, 2
- [25] Jianlong Yuan, Zelu Deng, Shu Wang, and Zhenbo Luo. Multi receptive field network for semantic segmentation. In *2020 IEEE Winter Conference on Applications of Computer Vision (WACV)*, pages 1883–1892. IEEE, 2020. 2

- [26] Hengshuang Zhao, Xiaojuan Qi, Xiaoyong Shen, Jianping Shi, and Jiaya Jia. Icnnet for real-time semantic segmentation on high-resolution images. In *Proceedings of the European conference on computer vision (ECCV)*, pages 405–420, 2018. 2, 8
- [27] Hengshuang Zhao, Jianping Shi, Xiaojuan Qi, Xiaogang Wang, and Jiaya Jia. Pyramid scene parsing network. In *Proceedings of the IEEE conference on computer vision and pattern recognition*, pages 2881–2890, 2017. 2